Synthesis of Farnesyl Diphosphate Analogues Containing Ether-Linked Photoactive Benzophenones and Their Application in Studies of Protein Prenyltransferases

Tammy C. Turek, Igor Gaon, and Mark D. Distefano*

Department of Chemistry, University of Minnesota, Minneapolis, Minnesota 55455

Corey L. Strickland

Department of Structural Chemistry, Schering-Plough Research Institute, Kenilworth, New Jersey 07033

distefan@chemsun.chem.umn.edu

Received July 15, 1999 (Revised Manuscript Received December 21, 2000)

Protein prenylation is a posttranslational lipid modification in which C_{15} and C_{20} isoprenoid units are linked to specific protein-derived cysteine residues through a thioether linkage. This process is catalyzed by a class of enzymes called prenyltransferases that are being intensively studied due to the finding that Ras protein is farnesylated coupled with the observation that mutant forms of Ras are implicated in a variety of human cancers. Inhibition of this posttranslational modification may serve as a possible cancer chemotherapy. Here, the syntheses of two new farnesyl diphosphate (FPP) analogues containing photoactive benzophenone groups are described. Each of these compounds was prepared in six steps from dimethylallyl alcohol. Substrate studies, inhibition kinetics, photoinactivation studies, and photolabeling experiments are also included; these experiments were performed with a number of protein prenyltransferases from different sources. A X-ray crystal structure of one of these analogues bound to rat farnesyltransferase illustrates that they are good substrate mimics. Of particular importance, these new analogues can be enzymatically incorporated into Ras-based peptide substrates allowing the preparation of molecules with photoactive isoprenoids that may serve as valuable probes for the study of prenylation function. Photoaffinity labeling of human protein geranylgeranyltransferase with ^{32}P-labeled forms of these analogues suggests that the C-10 locus of bound geranylgeranyl diphosphate (GGPP) is in close proximity to residues from the β-subunit of this enzyme. These results clearly demonstrate the utility of these compounds as photoaffinity labeling analogues for the study of a variety of protein prenyltransferases and other enzymes that employ FPP or GGPP as their substrates.

Introduction

Protein prenylation is a posttranslational lipid modification that involves attachment of a farnesyl (C_{15}) group from farnesyl diphosphate (FPP, **1**) or, more commonly, a geranylgeranyl (C_{20}) group from geranylgeranyl diphosphate (GGPP, **2**) to a specific cysteine residue of a protein substrate through a thioether linkage.

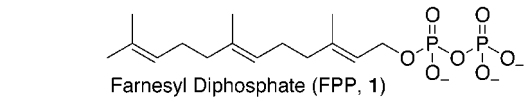

Farnesyl Diphosphate (FPP, **1**)

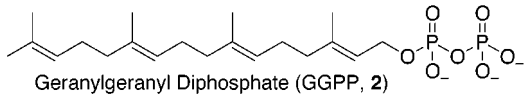

Geranylgeranyl Diphosphate (GGPP, **2**)

This process is catalyzed by protein prenyl transferases; at present, several enzymes have been identified from yeast and mammalian sources including two distinct protein farnesyl transferases (PFTase),[1,2] protein geranylgeranyltransferase type I (PGGTase-I),[3,4] and protein geranylgeranyltransferase type II (PGGTase-II).[5,6] Recently, there has been an explosion of interest in studying protein prenylation since oncogenic Ras is farnesylated and mutant forms have been detected in 30% of all human cancers[7] including 90% of pancreatic, 50% of colon, and 30% of lung cancers.[8] Since farnesylation is necessary for membrane association and cellular transformation of Ras oncoproteins, preventing this modification may eliminate the activity of oncogenic Ras and hence may serve as a possible cancer chemotherapy. This notion has generated an intense research effort to design inhibitors of PFTase as potential anticancer agents.[9−17] However, geranylgeranylation of cellular proteins is five

(1) Reiss, Y.; Goldstein, J. L.; Seabra, M. C.; Casey, P. J.; Brown, M. S. *Cell* **1990**, *62*, 81−88.
(2) Vogt, A.; Sun, J.; Qian, Y.; Tan-Chiu, E.; Hamilton, A. D.; Sebti, S. M. *Biochemistry* **1995**, *34*, 12398−12403.
(3) Moomaw, J. F.; Casey, P. J. *J. Biol. Chem.* **1992**, *267*, 17438−17443.
(4) Yokoyama, K.; Gelb, M. H. *J. Biol. Chem.* **1993**, *268*, 4055−4060.
(5) Seabra, M. C.; Goldstein, J. L.; Sudhof, T. C.; Brown, M. S. *J. Biol. Chem.* **1992**, *267*, 14497−14503.
(6) Armstrong, S. A.; Seabra, M. C.; Sudhof, T. C.; Goldstein, J. L.; Brown, M. S. *J. Biol. Chem.* **1993**, *268*, 12221−12229.
(7) Lerner, E. C.; Qian, Y.; Hamilton, A. D.; Sebti, S. M. *J. Biol. Chem.* **1995**, *270*, 26770−26773.
(8) McNamara, D. J.; Dobrusin, E.; Leonard, D. M.; Shuler, K. R.; Kaltenbronn, J. S.; Quin, J., II; Bur, S.; Thomas, C. E.; Doherty, A. M.; Scholten, J. D.; Zimmerman, K. K.; Gibbs, B. S.; Gowan, R. C.; Latash, M. P.; Leopold, W. R.; Przybranowski, S. A.; Sebolt-Leopold, J. S. *J. Med. Chem.* **1997**, *40*, 3319−3322.
(9) Buss, J. E.; Marsters, J. C. *Chem. Biol.* **1995**, *2*, 787−791.
(10) Gibbs, J. B.; Oliff, A.; Kohl, N. E. *Cell* **1994**, *77*, 175−178.

10.1021/jo991130x CCC: $20.00
Published on Web 04/14/2001

to ten times more prevalent than farnesylation in eukaryotic cells and tissues;[18] therefore, selective inhibition of PFTase is an important issue for inhibitors to be clinically useful.

Identifying active site residues of protein prenyltransferases may be useful in designing more potent inhibitors that are selective for PFTase and that do not affect other metabolic pathways. Photoaffinity labeling has provided important information concerning the active sites of these enzymes through investigating the substrate binding and recognition pattern. Incorporating a diazotrifluoropropionate (DATFP) cross-linking group into a FPP analogue, DATFP-GPP, specifically labeled the β subunit of human and yeast PFTase.[19−21] Preparation of a GGPP analogue, DATFP−FPP, labeled the β subunit of human and bovine brain PGGTase-I, implicating the involvement of the β subunit in prenyl substrate binding.[20,22] However, there are no reports in the literature of specific residues that have been identified to be important in isoprenoid binding using these DATFP photoactive analogues. This may be due to the difficulty in handling the diazoester moiety as well as the stability of the photolabel. Diazoester isoprenoid analogues are allylic esters with multiple pathways for degradation. Benzophenone analogues offer an attractive alternative to diazo- and azide-containing analogues due to their increased chemical stability, activation at higher wavelengths which are less damaging to the protein, ease of manipulation in ambient light, and preferential reactions with unreactive C−H bonds even in the presence of solvent and water molecules.[23] Ying and co-workers studied the PFTase protein substrate binding site by incorporating benzophenone groups into several peptide analogues.[24] When one benzophenone group was incorporated, they labeled the β subunit of human, rat, and bovine PFTase; with a peptide substrate analogue appended with two benzophenone moieties, they observed labeling of both the α and β subunit of these enzymes suggesting that the peptide binding site was located at the α/β subunit interface. Pellicena and colleagues also incorporated a benzophenone group into their peptide analogue and identified a specific amino acid on the α subunit of rat PFTase (rPFTase) important in peptide binding, demonstrating the utility of the benzophenone moiety at identifying important residues involved in substrate recognition.[25] Benzophenone-containing analogues have also been prepared and used to study several enzymes involved in the synthesis of isoprenoids including farnesyl synthase, hexaprenyl synthase, and undecaprenyl synthase.[26] In subsequent work, photolabeling with one of these compounds was used to show that component I of heptaprenyl synthase contained the isoprenoid diphosphate binding site.[27] We have previously reported work employing compounds incorporating photoactive benzophenones into FPP and GGPP analogues to identify the isoprenoid binding site and shown that the analogues specifically label the β subunit of yeast PFTase and human PGGTase-I. These results provide further evidence for this subunit's involvement in prenyl group recognition as was found with the DATFP analogues.[28,29] Recently, the X-ray crystal structure of rPFTase was solved, thus identifying the location of binding of FPP in the enzyme active site on the β subunit.[30−33] While there is substantial sequence identity among the mamalian PFTases (93% identity between the human and rat enzymes), only 37% amino acid identity between the β subunit of yeast PFTase and mammalian PFTases and 30% sequence similarity between the β subunit of PGGTase-I and mammalian PFTases exists.[19,34] Therefore, identifying similarities and differences between these enzymes in their prenyl substrate binding sites may facilitate the design and optimization of selective PFTase inhibitors.

In this paper, the syntheses of two new FPP analogues, **3a** and **3b**, are described along with substrate studies, inhibition kinetics, photoinactivation studies, and photolabeling experiments.

These experiments were performed on a number of protein prenyltransferases from different sources and the results from these findings are discussed. Crystallization of one of these analogues with rat farnesyltransferase illustrates that they are good substrate mimics. Of particular importance, these analogues can be enzymatically incorporated into Ras-based peptide substrates, allowing us to prepare molecules with photoactive isoprenoids that may serve as valuable probes for the study

(11) Gibbs, J. B.; Pompliano, D. L.; Mosser, S. D.; Rands, E.; Lingham, R. B.; Singh, S. B.; Scolnick, E. M.; Kohl, N. E.; Oliff, A. *J. Biol. Chem.* **1993**, *268*, 7617−7620.
(12) Manne, V.; Ricca, C. S.; Brown, J. G.; Tuomari, A. V.; Yan, N.; Patel, D.; Schmidt, R.; Lynch, M. J.; Ciosek, C. P.; Carboni, J. M.; Robinson, S.; Gordon, E. M.; Barbacid, M.; Seizinger, B. R.; Biller, S. A. *Drug Dev. Res.* **1995**, *34*, 121−137.
(13) Aoyama, T.; Satoh, T.; Yonemoto, M.; Shibata, J.; Nonoshita, K.; Arai, S.; Kawakami, K.; Iwasawa, Y.; Sano, H.; Tanaka, K.; Monden, Y.; Kodera, T.; Arakawa, H.; Suzuki-Takahashi, I.; Kamei, T.; Tomimoto, K. *J. Med. Chem.* **1998**, *41*, 143−147.
(14) Garcia, A. M.; Rowell, C.; Ackermann, K.; Kowalczyk, J. J.; Lewis, M. D. *J. Biol. Chem.* **1993**, *268*, 18415−18418.
(15) Lerner, E. C.; Qian, Y.; Blaskovich, M. A.; Fossum, R. D.; Vogt, A.; Sun, J.; Cox, A. D.; Der, C. J.; Hamilton, A. D. *J. Biol. Chem.* **1995**, *270*, 26802−26806.
(16) Breslin, M. J.; deSolms, S. J.; Giuliani, E. A.; Stokker, G. E.; Graham, S. L.; Pompliano, D. L.; Mosser, S. D.; Hamilton, K. A.; Hutchinson, J. H. *Bioorg. Med. Chem. Lett.* **1998**, *8*, 3311−3316.
(17) Manne, V.; Yan, N.; Carboni, J. M.; Tuomari, A. V.; Ricca, C. S.; Brown, J. G.; Andahazy, M. L.; Schmidt, R. J.; Patel, D.; Zahler, R.; Weinmann, R.; Der, C. J.; Cox, A. D.; Hunt, J. T.; Barbacid, M.; Seizinger, B. R. *Oncogene* **1995**, *10*, 1763−1779.
(18) Maltese, W. A. *FASEB J.* **1990**, *4*, 3319−3328.
(19) Omer, C. A.; Kral, A. M.; Diehl, R. E.; Prendergast, G. C.; Powers, S.; Allen, C. M.; Gibbs, J. B.; Kohl, N. E. *Biochemistry* **1993**, *32*, 5167−5176.
(20) Bukhtiyarov, Y. E.; Omer, C. A.; Allen, C. M. *J. Biol. Chem.* **1995**, *270*, 19035−19040.
(21) Edelstein, R. L.; Distefano, M. D. *Biochem. Biophys. Res. Commun.* **1997**, *235*, 377−382.
(22) Yokoyama, K.; McGeady, P.; Gelb, M. H. *Biochemistry* **1995**, *34*, 1344−1354.
(23) Dorman, G.; Prestwich, G. D. *Biochemistry* **1994**, *33*, 5661−5673.
(24) Ying, W.; Sepp-Lorenzino, L.; Cai, K.; Aloise, P.; Coleman, P. S. *J. Biol. Chem.* **1994**, *269*, 470−477.
(25) Pellicena, P.; Scholten, J. D.; Zimmerman, K.; Creswell, M.; Huang, C. C.; Miller, W. T. *Biochemistry* **1996**, *35*, 13494−13500.
(26) Marecak, D. M.; Horiuchi, Y.; Arai, H.; Shimonaga, M.; Maki, Y.; Koyama, T.; Ogura, K.; Prestwich, G. D. *Bioorg. Med. Chem. Lett.* **1997**, *7*, 1973−1978.
(27) Zhang, Y.-W.; Koyama, T.; Marecak, D. M.; Prestwich, G. D.; Maki, Y.; Ogura, K. *Biochemistry* **1998**, *37*, 13411−13420.
(28) Gaon, I.; Turek, T. C.; Weller, V. A.; Edelstein, R. L.; Singh, S. K.; Distefano, M. D. *J. Org. Chem.* **1996**, *61*, 7738−7745.
(29) Turek, T. C.; Gaon, I.; Gamache, D.; Distefano, M. D. *Bioorg. Med. Chem. Lett.* **1997**, *7*, 2125−2130.
(30) Park, H.-W.; Boduluri, S. R.; Moomaw, J. F.; Casey, P. J.; Beese, L. S. *Science* **1997**, *275*, 1800−1804.
(31) Dunten, P.; Kammlott, U.; Crowther, R.; Weber, D.; Palermo, R.; Birktoft, J. *Biochemistry* **1998**, *37*, 7907−7912.
(32) Long, S. B.; Casey, P. J.; Beese, L. S. *Biochemistry* **1998**, *37*, 9612−9618.
(33) Strickland, C. L.; Windsor, W. T.; Syto, R.; Wang, L.; Bond, R.; Wu, Z.; Schwartz, J.; Le, H. V.; Beese, L. S.; Weber, P. C. *Biochemistry* **1998**, *37*, 16601−16611.
(34) Mayer, M. L.; Caplin, B. E.; Marshall, M. S. *J. Biol. Chem.* **1992**, *267*, 20589−20593.

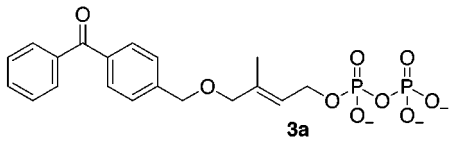

3a

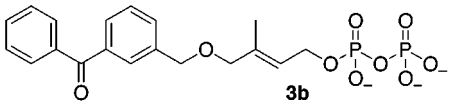

3b

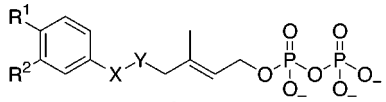

3c (R^1 = C_6H_5CO, R^2 = H, X = CO, Y = O)
3d (R^1 = H, R^2 = C_6H_5CO, X = CO, Y = O)
3e (R^1 = H, R^2 = C_6H_5CO, X = CO, Y = NH)

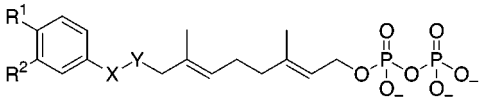

3f (R^1 = C_6H_5CO, R^2 = H, X = CO, Y = O)
3g (R^1 = H, R^2 = C_6H_5CO, X = CO, Y = O)
3h (R^1 = H, R^2 = C_6H_5CO, X = CO, Y = NH)
3i (R^1 = C_6H_5CO, R^2 = H, X = CH_2, Y = O)
3j (R^1 = H, R^2 = C_6H_5CO, X = CH_2, Y = O)

of prenylation function. These results clearly demonstrate these compounds' utility as photoaffinity labeling analogues for the study of a variety of protein prenyltransferases and other enzymes that employ FPP or GGPP as their substrates.

Results and Discussion

Design and Synthesis. Photoreactive analogues of FPP (**1**) and GGPP (**2**) are shown above. These analogues incorporate a *meta*- or *para*-substituted benzoylbenzyl photophore [4-BB-DMAPP (**3a**) and 3-BB-DMAPP (**3b**)] linked to a dimethylallyl unit via an acid stable ether linkage. They were designed based on the observation that these analogues had significant overlap with the structures of **1** and **2** as illustrated in Figure 1 where **1** and **2** are superimposed on **3b**. The compounds, **3a** and **3b**, were synthesized in six steps starting from commercially available dimethylallyl alcohol as shown in Scheme 1.

The hydroxyl group of dimethylallyl alcohol was protected by reaction with 3,4-dihydropyran and pyridinium *p*-toluenesulfonate (PPTs) to generate a tetrahydropyranyl ether in high yield. The resulting ether, **4**, was oxidized with *tert*-butyl hydroperoxide and catalytic H_2SeO_3 to yield **5** with *E*-stereoselectivity as evidenced by the disappearance of the C-4 methyl group in the ^{13}C NMR spectrum of **5**. Further support for *E*-stereoselectivity was achieved when a portion of **5** was reacted under Mitsunobu conditions with phthalimide to generate **6c**. As diagrammed in Scheme 1, NOE analysis of this compound shows a significantly stronger NOE between the C-2 vinyl proton and the C-4 methylene group (1.7%) than that observed between the C-2 vinyl proton and the C-3 methyl group (0.2%) consistent with a trisubstituted alkene with *E*-stereochemistry. Compound **5** was then treated with NaH and 4-(bromomethyl)benzophenone or 3-(bromomethyl)benzophenone to generate **6a** and **6b** in 78% and 68% yields, respectively. The requisite bromomethyl benzophenones were prepared by radical bromination with NBS using AIBN as the radical initiator following the procedure developed by Rajagopalan et al.[35] Deprotection of **6a** and **6b** was accomplished with PPTs in ethanol to give **7a** and **7b** in quantitative yield. In previous work with benzoylbenzoate esters, allylic alcohols similar to **7a** and **7b** were converted to the chlorides by treatment with *N*-chlorosuccinimide and dimethyl sulfide followed by pyrophosphorylation.[28,36] Subsequent work with benzoylbenzyl ethers used bromination instead of chlorination to obtain the activated species employed in the subsequent pyrophosphorylation.[37] In these experiments the brominated products were produced in higher yield than the earlier chlorides. Thus, bromination of **7a** and **7b** with PPh_3 and CBr_4 followed by displacement of the allylic bromides **8a** and **8b** with tris(tetra-*n*-butylammonium) hydrogen pyrophosphate generated **3a** and **3b** in 32% and 30% yields, respectively. Diphosphates **3a** and **3b** were purified by reversed-phase chromatography and characterized by ^1H NMR, ^{31}P NMR, UV, and HR-MALDI mass spectrometry. Compounds **3a** and **3b** are stable for several years when stored as lyophilized powders at −80 °C.

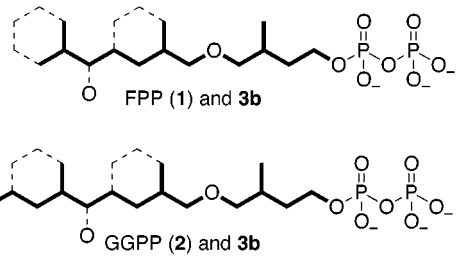

Superposition of FPP or GGPP with 3b

Figure 1. Superposition of **3b** with FPP (**1**) and GGPP (**2**). The structures of **1** and **2** are indicated in bold while the structure of **3b** is given as dashed bonds.

Substrate Studies. Initially, a continuous fluorescence assay using *N*-Ds-GCVIA (**9**) was employed to determine whether compounds **3a** and **3b** were substrates for yeast PFTase (yPFTase) and human PFTase (hPFTase).[38,39] When the natural substrate, **1**, was assayed, a time-dependent increase in fluorescence (approximately 10-fold) was observed; however, when **1** (10 μM) was replaced with 10 μM or 20 μM **3a** or **3b**, only a slight increase in fluorescence was seen, suggesting that these compounds were slow alternate substrates. To further explore the extent to which the analogues were substrates, the expected products of the enzymatic prenylation of **9** with **3a** and **3b** were prepared by chemical synthesis using the method of Xue et al.[40] illustrated in Scheme 2.

The chemically synthesized products **10a** and **10b** were purified by reversed-phase HPLC and analyzed by ESI

(35) Rajagopalan, K.; Chavan, A. J.; Haley, B. E.; Watt, D. S. *J. Biol. Chem.* **1993**, *268*, 14230−14238.
(36) Turek, T. C.; Gaon, I.; Distefano, M. D. *Tetrahedron Lett.* **1996**, *37*, 4845−4848.
(37) Gaon, I.; Turek, T. C.; Distefano, M. D. *Tetrahedron Lett.* **1996**, *37*, 8833−8836.
(38) Pompliano, D. L.; Gomez, R. P.; Anthony, N. J. *J. Am. Chem. Soc.* **1992**, *114*, 7945−7946.
(39) Bond, P. D.; Dolence, J. M.; Poulter, C. D. *Methods Enzymol.* **1995**, *250*, 30−43.
(40) Xue, C.-B.; Becker, J. M.; Naider, F. *Tetrahedron Lett.* **1992**, *33*, 1435−1438.

Scheme 1

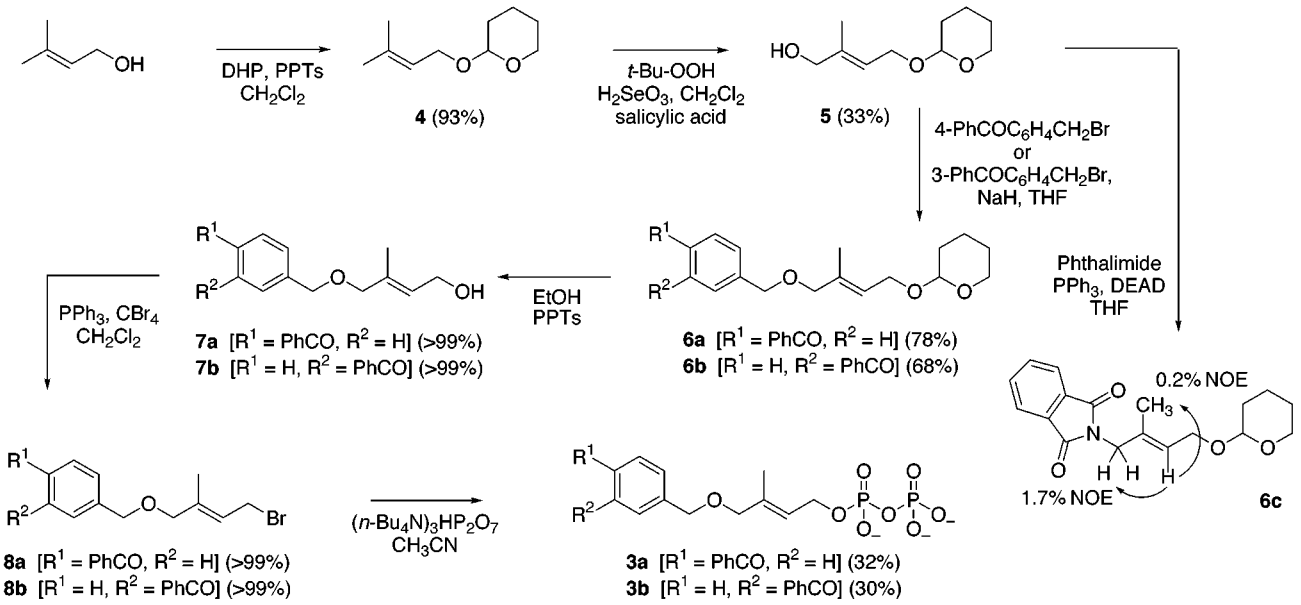

Scheme 2

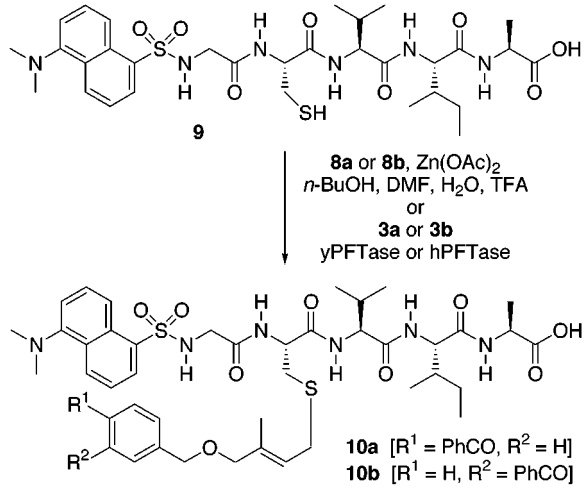

MS and ESI MS/MS to reveal the fragmentation pattern. The ESI MS and ESI MS/MS for **10a** are displayed in Figures 2A and 2B.

For **10a**, an $[M + H]^+$ peak of 973.2 was observed as well as the doubly charged ion $[M + 2H]^{2+}$ at 487.0. Similar peaks and values were obtained for **10b** (data not shown). Interestingly, the chemically synthesized products show b-type fragmentation up to the modified cysteine amino acid at which point the C−S bond of the β carbon cysteine is cleaved removing the entire analogue including the sulfur atom. Another important fragmentation observed is the loss of the dansyl group and cleavage of the C−S bond formed between the cysteine thiol and the benzoylbenzyl adduct. With the authentic products characterized, the products from the large-scale enzymatic reactions (10 mL) between **3a** or **3b** and **9** with yPFTase or hPFTase were analyzed by HPLC and compared to those of the chemically synthesized products. The HPLC chromatograms monitored by UV and fluorescence are shown in Figures 3A and 3B for the reaction between **3a** and **9** with yPFTase.

The fluorescent product peaks, with elution times similar to those of the chemically synthesized products were collected, concentrated, and analyzed by ESI MS and ESI MS/MS. The ESI MS for **10a** obtained via yPFTase (Figure 4A) showed an $[M + H]^+$ peak of 973.4 as well as the an $[M + 2H]^{2+}$ at 486.8 giving a calculated $[M]^+$ value of 971.99 ± 0.57. For **10b** (Figure 4B), we observed an $[M + H]^+$ peak at 973.4 and the doubly charged ion at 487.0 giving a $[M]^+$ value of 972.17 ± 0.31 corresponding to the expected peptide products in Scheme 2.

The ESI MS/MS for the enzymatic reactions (data not shown) gave similar fragmentation patterns as seen with the authentic products. For the enzymatic reactions

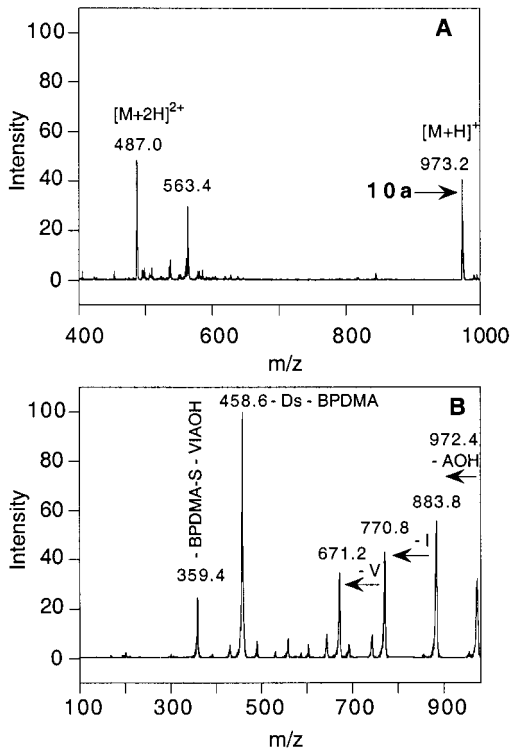

Figure 2. ESI MS and ESI MS/MS of chemically synthesized product **10a**. Panel A: ESI MS of *Ds*-GC(4-BBDMA)VIA. Panel B: ESI MS/MS of *Ds*-GC(4-BBDMA)VIA.

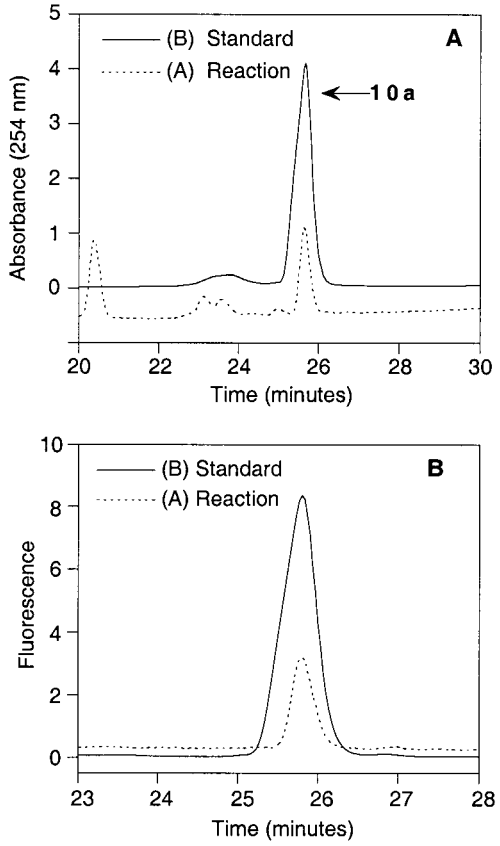

Figure 3. HPLC analysis of reactions containing yPFTase, **9**, and **3a**. Panel A: UV analysis, chromatogram A is from a 10 mL reaction mixture containing **9** and **3a**. Chromatogram B is from a sample of chemically synthesized **10a**. The amount of **10a** injected is equal to the amount of product that would be formed in the enzymatic reaction assuming 100% conversion. Panel B: fluorescence (480−520 nm) detection, chromatogram A is from a 10 mL reaction mixture containing **9** and **3a**. Chromatogram B is from a sample of chemically synthesized **10a**. The amount of **10a** injected is equal to the amount of product that would be formed in the enzymatic reaction assuming 100% conversion.

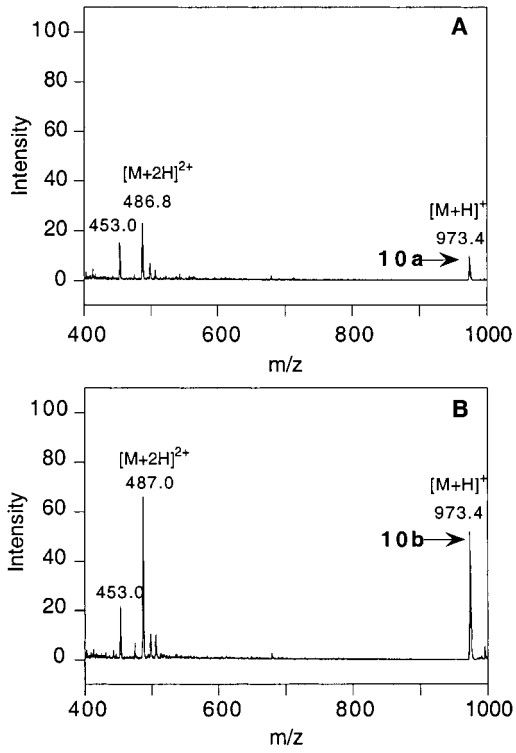

Figure 4. ESI MS of the enzymatic prenylation of yPFTase, **9**, and **3a** or **3b**. Panel A: ESI MS from a 10 mL reaction mixture containing **9** and **3a** with yPFTase and generation of the enzymatic product *Ds*-GC(4-BBDMA)VIA. Panel B: ESI MS from a 10 mL reaction mixture containing **9** and **3b** with yPFTase and generation of the enzymatic product *Ds*-GC(3-BBDMA)VIA.

containing hPFTase, the results are similar to those obtained with yPFTase and the chemically synthesized products, giving a $[M]^+$ peak of 972.36 ± 0.17 for **10a** and a $[M]^+$ peak of 972.35 ± 0.14 for **10b** as well as similar ESI MS/MS patterns (data not shown). To quantify the amount of product formed in all four cases, the chemically synthesized products were injected in an amount equal to that formed in the enzymatic reactions assuming 100% conversion and the peak areas integrated using fluorescence detection. The amount of enzymatic product formed by yPFTase was 23% for **10a** and 81% for **10b**; however, the large scale reactions were performed with 18-fold greater amounts of enzyme and were allowed to react for 6-fold longer times than would be required with the natural substrate, FPP. For **10a**, enzymatically prepared by hPFTase, a yield of 8% was achieved and for **10b** a 20% yield was observed. These reactions were accomplished with 4-fold greater amounts of enzyme and reacted for 6-fold longer reaction times than required with FPP; thus, these analogues are poor substrates for the human enzyme. It is useful to compare the results described here with earlier observations with related analogues. With the C_{10} benzoylbenzoate ester analogues, **3f** and **3g**, and yPFTase, the yields of product formed were less than 1%, and hence the analogues were not substrates for yPFTase; therefore, these results indicate that the shorter chain benzoylbenzyl ether analogues more closely mimic the natural substrate **1** than the longer C_{10} ester analogues.[28] Based on the above discussion, it is clear that **3a** and **3b** are not efficient alternate substrates. However, using larger amounts of enzyme and long reaction times it is possible to obtain efficient incorporation of **3b** into a peptide and presumably into a protein. This provides a means of preparing proteins that contain photoactive isoprenoids which could be useful in studying the role of protein prenylation.

Inhibition Kinetics. Since formation of products **10a** and **10b** from the enzymatic reaction of **3a** and **3b** with **9** by yPFTase and hPFTase were undetected using low concentrations PFTase (5.1 nM) in the fluorescence assay, their rates of reaction are negligible compared to that of FPP under typical assay conditions; therefore, the fluorescence assay was used to measure the inhibition kinetics of PFTase by analogues **3a** and **3b**. The rate of yPFTase- and hPFTase-catalyzed farnesylation of *N*-Ds-GCVIA was measured in the presence of fixed concentrations of FPP at varying concentrations of **3a** and **3b**. The concentrations of **3a** and **3b** used were chosen based on their IC_{50} values (Table 1) which were determined in preliminary experiments to be 12 μM and 3.4 μM. Double reciprocal plots of the data for **3a** with yPFTase (Figure 5) and **3a** with hPFTase (Figure 6) both give patterns of lines that intersect on the $1/v$ axis, consistent with competitive inhibition with respect to FPP.

Similar results were achieved with **3b** using the yeast

Table 1. Summary of Inhibition Parameters for Benzophenone-Based Photoaffinity Labeling Analogues with Yeast and Human PFTases

compd	yFPTase IC_{50} (μM)	yFPTase K_I (μM)	yFPTase photoinact after 12 h (%)	hFPTase IC_{50} (μM)	hFPTase K_I (μM)
3a	12 ± 0.55	1.0 ± 0.12	51	2.3 ± 0.32	0.34 ± 0.04
3b	3.4 ± 0.41	0.61 ± 0.14	53	3.6 ± 0.18	0.61 ± 0.14
3c[a]	5.1	2.9	74	–	–
3d[a]	2.0	0.96	63	–	–
3e[b]	37	6.0	–	–	–
3f[c]	3.0	0.91	44	–	–
3g[c]	2.3	0.38	30	–	–
3h[b]	3.7	0.70	–	–	–
3i[d]	1.6	0.045	40	–	–
3j[d]	0.85	0.049	40	–	–
FPP		0.075 (K_D)[e]			0.012 (K_D)[f]

[a] From ref 33. [b] From ref 27. [c] From ref 26. [d] From ref 34. [e] From ref 20. [f] From ref 21.

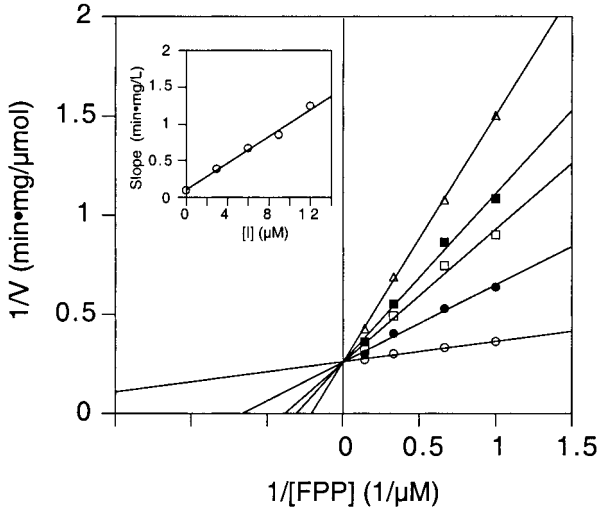

Figure 5. Double reciprocal plot showing the competitive inhibition of yPFTase by **3a**. The concentrations of **3a** are as follows: (○) 0 μM, (●) 3.0 μM, (□) 6.0 μM, (■) 9.0 μM, (△) 12 μM. Inset: replot of slopes from double reciprocal plot versus [**3a**].

and human enzymes (data not shown). The rates were further analyzed by the Eadie−Hofstee method to determine K_i values for each inhibitor. A K_i of 1.0 μM was calculated for **3a**, while **3b** gave a K_i value of 0.61 μM using yPFTase. For inhibition studies on hPFTase, a K_i of 0.34 μM for **3a** and 0.61 μM for **3b** were obtained. By comparing these findings to values obtained with other analogues studied (Table 1), it is clear that structural features within the analogues affect their binding affinities for the protein prenyltransferases. This includes variations in the isoprenoid chain length, type of linkage (amide, ester or ether), and benzophenone regiochemistry (*meta*- versus *para*-substituted benzophenone). Comparison of K_i values of **3a** and **3b** with yPFTase and hPFTase reveals small differences in their binding affinity. For all yPFTase K_i values, the *meta*-linked analogues are more efficient or at least as efficient as the *para*-linked analogues at binding; however, with hPFTase a change in efficiency occurs, suggesting that the shapes of the isoprenoid binding pocket of these two enzymes may be different. By comparing the C_5 ether-linked analogues **3a** and **3b** with the C_5 ester-linked compounds **3c** and **3d**, and amide-linked analogue, **3e**, it can be seen that the carbonyl groups diminish the extent of binding. This

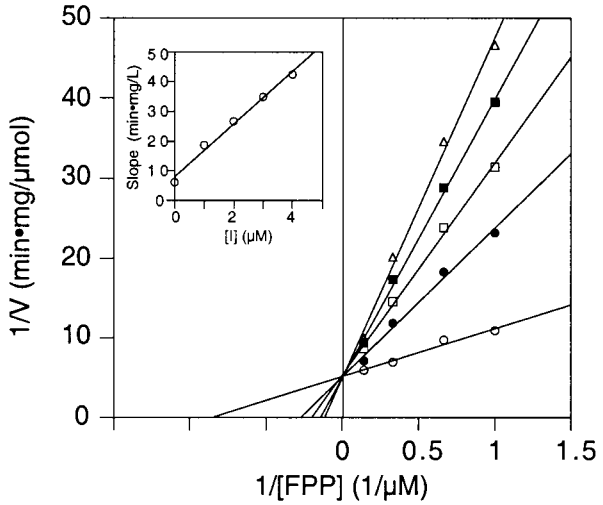

Figure 6. Double reciprocal plot showing the competitive inhibition of hPFTase by **3a**. The concentrations of **3a** are as follows: (○) 0 μM, (●) 1.0 μM, (□) 2.0 μM, (■) 3.0 μM, (△) 4.0 μM. Inset: replot of slopes from double reciprocal plot versus [**3a**].

may be due to steric interactions with the protein or it may reflect the greater rigidity of the ester and amide-containing analogues. Comparison of K_i values of **3a** and **3b** with those for **3i** and **3j** indicates that the presence of the second isoprene unit significantly increases the affinity of these compounds for PFTase. However, this enhanced affinity is accompanied by a commensurate decrease in incorporation efficiency that is consistent with size limitations imposed by the PFTase isoprenoid binding pocket as evidenced by the X-ray crystal structure. As we have noted with previous compounds,[28] the diphosphate functionality present in **3a** and **3b** is essential for binding. No inhibition at concentrations of up to 20 μM was observed with the free alcohols **7a** and **7b**.

X-ray Crystallographic Studies. To gain additional insight into how these isoprenoid diphosphate analogues interact with a prenyltransferase, crystals of **3a** bound to rPFTase were obtained, and the structure of the resulting complex was determined via X-ray diffraction experiments. Electron density maps clearly show the bound conformation and location of **3a** in the PFTase active site cavity. The presence of the higher molecular weight phosphate atoms in the molecule assists in unambiguous definition of the binding mode. Comparison of the protein in the structure of the FPT:**3a** complex and the FPT:FPP:SCH66336 ternary complex shows a 0.2 Å rms deviation for all protein atoms, indicating minimal movement of protein side-chains.[33,41] The position of the diphosphate atoms are well conserved between **3a** and FPP while the benzophenone occupies the binding site of the second and third isoprenoid units of FPP. A superposition of **3a** and FPP in the isoprenoid binding pocket of rPFTase is shown in Figure 7. These structural data combined with the observations that **3a** is a slow alternative substrate and modest inhibitor suggest that **3a** is a good structural analogue of FPP.

(41) Strickland, C. L.; Weber, P. C.; Windsor, W. T.; Wu, Z.; Le, H. V.; Albanese, M. M.; Alvarez, C. S.; Cesarz, D.; Rosario, J. d.; Deskus, J.; Mallams, A. K.; Njoroge, F. G.; Piwinski, J. J.; Remiszewski, S.; Rossman, R. R.; Taveras, A. G.; Vibulbhan, B.; Doll, R. J.; Girijavallabhan, V. M.; Ganguly, A. K. *J. Med. Chem.* **1999**, *42*, 2125−2135.

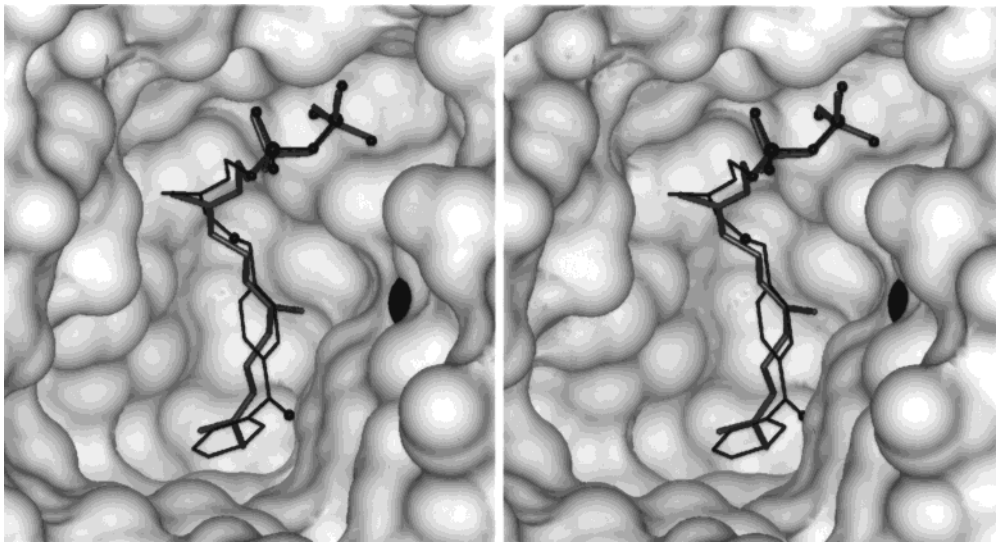

Figure 7. Stereoview of the binding of **3a** (black) compared with FPP (gray) to rPFTase. The non-carbon atoms of **3a** are shown as small spheres. The rPFTase active site zinc is shown as a large black spot on the enzyme surface.

Photoinactivation of yPFTase. Compounds **3a** and **3b** were tested for their ability to inactivate yPFTase upon UV irradiation at 350 nm by performing experiments containing mixtures of the inhibitors and the enzyme, withdrawing aliquots at regular intervals, and assaying the resulting samples for enzyme activity (data not shown). Samples containing enzyme alone were irradiated for up to 12 h with a low pressure 350 nm lamp with no appreciable loss in enzyme activity. In contrast, samples irradiated for 2 h containing **3a** or **3b** at saturating concentrations resulted in a 12% decrease in enzyme activity with **3a** and a 9% decrease with **3b**. Furthermore, the enzyme was protected from inactivation by **3a** or **3b**; upon addition of **1** (100 μM), only 8% inactivation was observed with **3a** and 1% inactivation was obtained with **3b** after 2 h irradiation. Greater levels of inactivation were achieved with longer incubation times. Photolysis of yPFTase in the presence of **3a** resulted in 51% inactivation after 12 h and with **3b** resulted in 53% inactivation. It should be noted that no inactivation occurred when yPFTase was incubated with **3a** or **3b** in the dark, and that inactivation ceased when irradiation of the reaction mixtures was stopped. Plots of enzyme activity versus irradiation time in the presence of **3a** or **3b** at saturating concentrations (data not shown) lead to values for the apparent k_{inact} of 0.060 ± 0.002 h^{-1} and 0.061 ± 0.006 h^{-1}, respectively. These values are relatively slow; for example Colman and co-workers reported a value of 15 h^{-1} for k_{inact} for photoinactivation of glutathione S-transferase by a benzophenone-containing inhibitor.[42] While this may be due in part to the low intensity of the UV source used in our experiments, we believe it is also related to the type of residues that comprise the FPP binding site in PFTase. It is interesting to note from the crystal structure of the rPFTase-**3a** complex that all of the residues within 6 Å of the benzophenone carbonyl group (W102, W106, W303, Y361, and Y365) contain aromatic side chains. Hydrogens attached to sp^2-hybridized carbons are among the least reactive C−H bonds in proteins.[23] From the structure of the protein complex shown in Figure 7, it is also apparent that the two aromatic rings of the benzophenone chromophore in **3a** are orthogonal to one another. Thus, for light absorption at 350 nm to occur, the molecule must adopt a planar, higher energy conformation, thereby further decreasing the rate of photoinactivation. Comparison of photoinactivation results (Table 1) of yPFTase in the presence of **3a** and **3b** to **3i** and **3j** indicates these shorter chain ether analogues have a slightly higher cross-linking efficiency. Comparing these analogues to the C_5 ester compounds **3c** and **3d**, which gave the best cross-linking efficiencies reported to date for all our analogues, suggests that the conformational rigidity provided by the ester group may be important in fixing the analogues in the active site area relative to the C_5 ether analogues which have greater rotational flexibility. Additional crystallographic studies of the ester complexes and rPFTase will be useful in clarifying this issue.

Photolabeling of Protein Prenyltransferases with [^{32}P]3a and [^{32}P]3b. To examine the ability of **3a** and **3b** to label yPFTase, hPFTase, and hPGGTase-I upon photolysis, the radiolabeled analogues [^{32}P]**3a** and [^{32}P]-**3b** were synthesized and purified using a method previously described,[43] adapted from a procedure developed by Bukhtiyarov.[20] Photolysis of prenyltransferases (380 nM) with 350 nm light for 2 h in the presence of [^{32}P]**3a** or [^{32}P]**3b** at concentrations of [^{32}P]**3a** and [^{32}P]**3b** that were 10-fold above K_i for yPFTase resulted in preferential labeling of the β subunit for each enzyme (Figure 8: yPFTase and [^{32}P]**3a**, Figure 9: hPFTase and [^{32}P]**3b**, and Figure 10: hPGGTase-I and [^{32}P]**3a**; lane 2′ in each Figure).

Addition of the natural substrate, **1** or **2**, to the photolysis reactions containing [^{32}P]**3a** or [^{32}P]**3b** resulted in protection from labeling (Figure 8: yPFTase and [^{32}P]-**3a**, Figure 9: hPFTase and [^{32}P]**3b**, and Figure 10: hPGGTase-I and [^{32}P]**3a**; lane 3′ in each Figure). To quantitate the relative labeling efficiencies of each subunit for each reaction, phosphorimaging analysis was employed. For photolabeling of yPFTase with [^{32}P]**3a** and [^{32}P]**3b**, the β subunit was labeled 1.6-fold over the α subunit. Addition of **1** in the photolysis reaction resulted

(42) Wang, J.; Bauman, S.; Colman, R. F. *Biochemistry* **1998**, *37*, 15671−15679.

(43) Turek, T. C.; Gaon, I.; Distefano, M. D. *J. Labeled Compds. Radiopharm.* **1997**, *39*, 139−146.

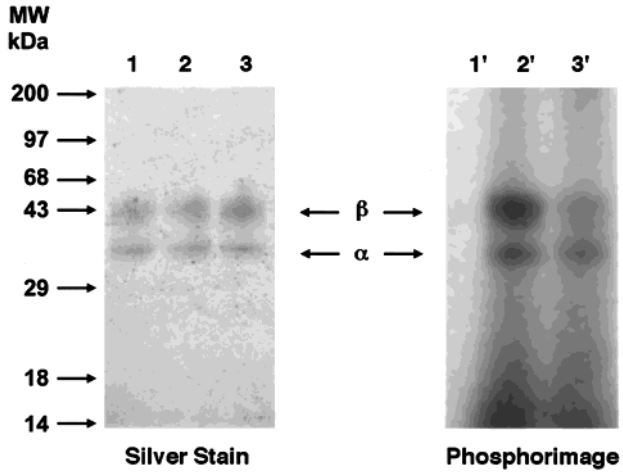

Figure 8. Analysis of photolabeling of yPFTase with [^{32}P]**3a** by SDS−PAGE. Lanes 1 and 1′ contain samples of yPFTase and [^{32}P]**3a** which were not irradiated. Lanes 2 and 2′ contain samples of yPFTase irradiated at 350 nm in the presence of [^{32}P]**3a**. Lanes 3 and 3′ contain samples of yPFTase irradiated in the presence of [^{32}P]**3a** and **1**. Lanes 1, 2, and 3 show silver-stained proteins. Lanes 1′, 2′, and 3′ show the radiolabeled proteins.

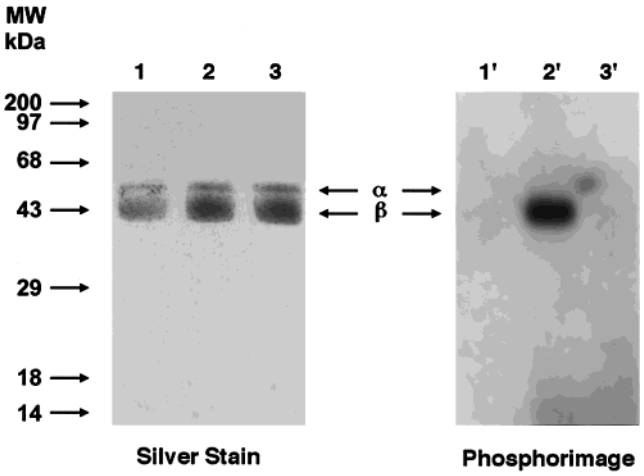

Figure 9. Analysis of photolabeling of hPFTase with [^{32}P]**3b** by SDS−PAGE. Lanes 1 and 1′ contain samples of hPFTase and [^{32}P]**3b** which were not irradiated. Lanes 2 and 2′ contain samples of hPFTase irradiated at 350 nm in the presence of [^{32}P]**3b**. Lanes 3 and 3′ contain samples of hPFTase irradiated in the presence of [^{32}P]**3b** and **1**. Lanes 1, 2, and 3 show silver-stained proteins. Lanes 1′, 2′, and 3′ show the radiolabeled proteins.

in a 3.3-fold decrease in β subunit labeling and a 1.4-fold decrease in α subunit labeling for [^{32}P]**3a**. Similar experiments with [^{32}P]**3b** resulted in a 4.0-fold decrease in β subunit labeling and a 3.1-fold decrease in α subunit labeling. In the case of hPFTase photolabeling by [^{32}P]-**3a** and [^{32}P]**3b**, the β subunit was labeled 4.3-fold and 8.3-fold over the α subunit, respectively. Addition of **1** resulted in 2.0-fold decrease in β labeling and a 3.8-fold decrease in α labeling for [^{32}P]**3a**. A 6.2-fold decrease in β labeling and a 1.0-fold decrease in α labeling occurred with [^{32}P]**3b** in the presence of **1**. In general, the labeling using the *meta*-substituted analogue, **3b**, appears to be more specific. Total labeling of yPFTase ($\alpha + \beta$) in the presence of **3b** and **1** decreased to 28% of that obtained in the absence of the competitor, **1**. This is in rough

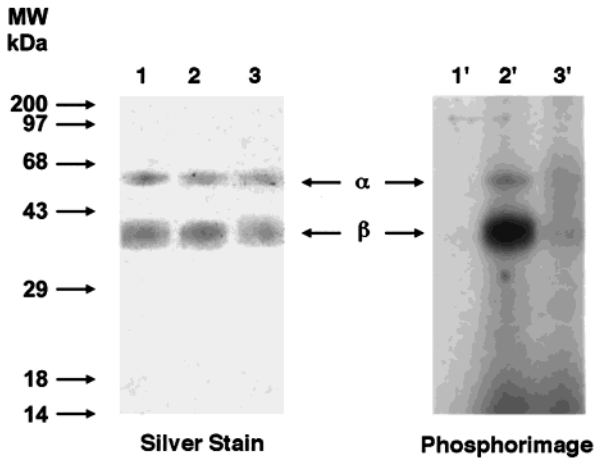

Figure 10. Analysis of photolabeling of hPGGTase-I with [^{32}P]-**3a** by SDS−PAGE. Lanes 1 and 1′ contain samples of hPGGTase-I and [^{32}P]**3a** which were not irradiated. Lanes 2 and 2′ contain samples of hPGGTase-I irradiated at 350 nm in the presence of [^{32}P]**3a**. Lanes 3 and 3′ contain samples of hPGGTase-I irradiated in the presence of [^{32}P]**3a** and **2**. Lanes 1, 2, and 3 show silver-stained proteins. Lanes 1′, 2′, and 3′ show the radiolabeled proteins.

agreement with the extent of protection obtained in the photoinactivation experiments described above; in that case inactivation in the presence of **3b** and **1** decreased to 11% of that obtained in the absence of the **1**. In contrast, total labeling of yPFTase in the presence of **3a** and **1** decreased to only 54% of that obtained in the absence of the competitor. Again rough agreement with the extent of protection obtained in the photoinactivation experiments was observed; inactivation in the presence of **3a** and **1** decreased to 75% (or 50% in a different experiment) of that obtained in the absence of the **1**. Interestingly, the greater labeling specificity obtained with **3b** compared with **3a** (in terms of protection from labeling of yPFTase in the presence of **1**) was also observed in photolabeling experiments with hPFTase. Total labeling of hPFTase in the presence of **3b** and **1** decreased to 25% of that obtained in the absence of the **1** while a decrease to 44% was observed in similar experiments performed with **3a** and **1**. Last, photolysis of hPGGTase-I by [^{32}P]**3a** and [^{32}P]**3b** gave 8.0-fold labeling of β over α with [^{32}P]**3a** and a 6.4-fold β over α subunit labeling for [^{32}P]**3b**. Addition of **2** in the photolysis reaction with [^{32}P]**3a** resulted in a 8.1-fold decrease in β subunit labeling and a 1.3-fold decrease in α subunit labeling. Similar experiments with [^{32}P]**3b** resulted in a 6.5-fold decrease in β subunit labeling and a 1.3-fold decrease in α subunit labeling. These results suggest that the β subunit is involved in prenyl group recognition for all three enzymes and are consistent with our work previously reported using other benzophenone analogues with yPFTase and hPGGTase-I as well as work obtained using other photoactive analogues on all three enzymes.[19−22,28,29,44] Moreover, these data provide additional information concerning the isoprenoid binding sites of these enzymes. Earlier work with benzophenone analogues prepared from geraniol (**3f**−**j**) suggested that the C-14 locus of GGPP was proximal to the β subunit in the isoprenoid/PGGTase complex as shown in Figure 11. This is based on the observation that C-14 of GGPP is close to the ketone carbon of **3f**−**j** when these analogues are superimposed with GGPP. In the present

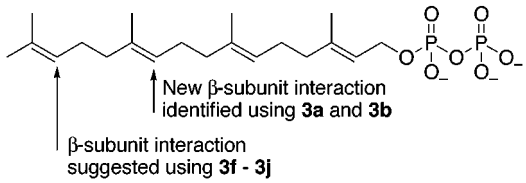

Figure 11. Model for the interaction of benzophenone-based photoaffinity labeling analogues with prenyltransferases.

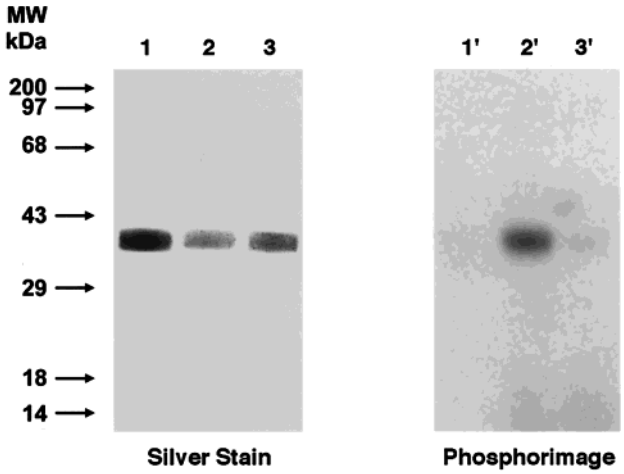

Figure 12. Analysis of photolabeling of FPP synthase with [^{32}P]**3b** by SDS−PAGE. Lanes 1 and 1′ contain samples of FPP synthase and [^{32}P]**3b** which were not irradiated. Lanes 2 and 2′ contain samples of FPP synthase irradiated at 350 nm in the presence of [^{32}P]**3b**. Lanes 3 and 3′ contain samples of FPP synthase irradiated in the presence of [^{32}P]**3b** and **1**. Lanes 1, 2, and 3 show silver-stained proteins. Lanes 1′, 2′, and 3′ show the radiolabeled proteins.

study, the subunit labeling results obtained with **3a** and **3b** suggest that the C-10 regions of FPP and GGPP also interact with the respective β subunits of these enzymes. While this was already known with PFTase (from the X-ray structure), it is a new piece of structural information in the case of hPGGTase.

Photolabeling of FPP Synthase with [^{32}P]3a and [^{32}P]3b. FPP synthase catalyzes the condensation of isopentenyl pyrophosphate and either dimethylallyl pyrophosphate or geranyl pyrophosphate generating FPP (**1**). Although this enzyme catalyzes a similar prenyl transfer reaction to those catalyzed by prenyltransferases, there is little sequence homology between these enzymes.[19] To determine if [^{32}P]**3a** and [^{32}P]**3b** are capable of photolabeling FPP synthase, the enzyme (465 nM) was irradiated with 350 nm light for 2 h in the presence of [^{32}P]**3a** (13 μM) or [^{32}P]**3b** (6.6 μM) which resulted in labeling FPP synthase (Figure 12; lane 2′, labeling with [^{32}P]**3b**).

Addition of **1**, to the photolysis reactions containing [^{32}P]**3a** or [^{32}P]**3b** resulted in protection from labeling (Figure 12; lane 3′, labeling with [^{32}P]**3b**). To quantitate the relative labeling efficiencies for each reaction, phosphorimaging analysis was employed (data not shown). For photolabeling with [^{32}P]**3a**, addition of **1** in the photolysis reaction resulted in a 8.1-fold decrease in labeling and for [^{32}P]**3b** resulted in a 12-fold decrease in labeling. From these studies it is apparent that these analogues are capable of binding other enzymes and should be useful for studying other enzymes that utilize isoprenoid diphosphates as substrates.

Conclusion

Compounds **3a** and **3b** are analogues of FPP that can be efficiently prepared in six steps from dimethylallyl alcohol. Both compounds are modest competitive inhibitors of yPFTase and hPFTase, but at higher enzyme concentrations and longer reaction times **3b** can be effectively transferred to a peptide substrate. A crystal structure with rat farnesyltransferase illustrates that **3a** is a good substrate mimic. Photolysis of **3a** and **3b** with several different prenyltransferases results in the specific labeling of these proteins and suggests that the C-10 loci of FPP and GGPP are bound at sites on the β subunits of their respective transferases. Analogues **3a** and **3b** also label FPP synthase. Given their ease of synthesis, higher stability relative to ester analogues and good photolabeling properties, these compounds should be useful for a variety of studies with other isoprenoid-utilizing enzymes.

Experimental Section

Methods and Materials. All reactions were conducted under dry nitrogen and stirred magnetically. Analytical TLC was performed on precoated (0.25 mm) silica gel 60F-254 plates purchased from E. Merck. Visualization was accomplished under UV irradiation or by subjecting the plates to ethanolic phosphomolybdic acid solutions followed by heating. Flash chromatography silica gel (60−120 mesh) was obtained by E. M. Science. CH_2Cl_2 and CH_3CN were distilled from CaH_2, and THF was distilled from sodium/benzophenone ketyl. Trifluoroacetic acid (TFA) was purchased from Fisher. NMR *J* values are given in Hz. UV spectra were obtained using a Hewlett-Packard 8452A spectrophotometer, and fluorescence measurements were performed with a Perkin-Elmer LS 50B luminescence spectrometer. HPLC analysis was carried out using a Beckman Model 127/166 instrument equipped with a diode array UV detector and a Beckman 6300A fluorescence detector (305−395 nm excitation filter and 480−520 nm emission filter). Preparative HPLC separations were performed with a Rainin Dynamax Microsorb C_{18} column (2.14 × 25 cm with a 5 cm guard column), while analytical separations employed a Rainin Dynamax Microsorb C_{18} column (5 μm, 4.6 × 250 mm with a 15 mm guard column). Phosphorimaging analysis was performed with a Molecular Dynamics 445 SI Phosphorimager. Sep-pak columns were obtained from Waters and Dowex 50W-X8 resin was obtained from Bio-Rad. *N*-dansylglycine was purchased from Sigma. *N*-Dansyl-GCVIA was purchased from Bio-Synthesis, Inc. and purified by reversed-phase preparative HPLC. [^{32}P]H_3PO_4 (specific activity 8500−9120 Ci/mmol) was obtained from DuPont NEN. *E. coli* DH5α/pGP114 and purified FPP synthase were generous gifts from C. D. Poulter, Department of Chemistry, University of Utah. *E. coli* BL21(DE3)/pRD577 and purified human PFTase were provided generously to us from C. A. Omer, Merck Research Laboratories, and P. J. Casey, Department of Molecular Cancer Biology, Duke University Medical Center, respectively.

1-[(Tetrahydro-2H-pyran-2-yl)oxy]-3-methyl-2-butene (4). To a solution of 3-methyl-2-buten-1-ol (3.4 g, 40 mmol) in CH_2Cl_2 (40 mL) were added 3,4-dihydropyran (5.0 g, 60 mmol) and PPTs (1.0 g, 4.0 mmol); the resulting solution was stirred for 4 h at room temperature. The reaction mixture was partially evaporated, diluted with Et_2O, and washed with saturated $NaHCO_3$. The organic layer was dried over Na_2SO_4 and concentrated to yield a colorless oil (6.3 g, 93%). R_f 0.62 (silica gel, toluene/EtOAc, 5:2, v/v); ^{1}H NMR (200 MHz, $CDCl_3$): δ 1.40−1.85 (m, 6H), 1.64 (s, 3H), 1.70 (s, 3H), 3.40−3.51 (m, 1H), 3.79−3.86 (m, 1H), 3.92 (dd, 1H, J = 6.0, 12.0), 4.17 (dd, 1H, J = 6.0, 12.0), 4.58 (t, 1H, J = 4.0), 5.28 (t, 1H, J = 6.0); ^{13}C NMR (50.3 MHz, $CDCl_3$): δ 17.7, 19.5 (primary), 25.2, 25.6, 30.5, 62.0, 63.4 (secondary), 97.6, 120.8 (tertiary), 136.6

(quaternary); LR−CI MS (NH_3): *m/z* (relative intensity) 85.07 (100), 103.07 (34), 170.13 ($[M]^+$, 14), 171.14 ($[M + H]^+$, 40); HR−CI MS: for $C_{10}H_{18}O_2$ $[M]^+$, calcd 170.1302, found 170.1299, for $C_{10}H_{19}O_2$ $[M + H]^+$, calcd 171.1380, found 171.1387.

(*E*)-1-[(Tetrahydro-2H-pyran-2-yl)oxy]-3-methyl-2-buten-4-ol (5). Compound **4** (6.3 g, 37 mmol) and *tert*-butyl hydroperoxide (14 mL, 120 mmol) were stirred in the presence of H_2SeO_3 (480 mg, 3.4 mmol) and salicylic acid (480 mg, 3.4 mmol) in CH_2Cl_2 (40 mL) for 10 h at room temperature. The CH_2Cl_2 was removed under reduced pressure and the *tert*-butyl hydroperoxide was removed by repeated washing with toluene. The residue was dissolved in Et_2O, washed with $NaHCO_3$ to remove H_2SeO_3, dried over Na_2SO_4, and filtered. The organic layer was concentrated and the crude product purified by flash chromatography on silica gel (toluene/EtOAc, 5:2, v/v) to afford compound **5** as a colorless oil (2.3 g, 33%). R_f 0.25 (silica gel, toluene/EtOAc, 5:2, v/v); ^{1}H NMR (300 MHz, $CDCl_3$): δ 1.48−1.81 (m, 6H), 1.65 (s, 3H), 3.44−3.49 (m, 1H), 3.80−3.86 (m, 1H), 3.97 (s, 2H), 4.02 (dd, 1H, J = 6.0, 12.0), 4.24 (dd, 1H, J = 6.0, 12.0), 4.44 (t, 1H, J = 4.0), 5.58 (t, 1H, J = 6.0); ^{13}C NMR (75.4 MHz, $CDCl_3$): δ 13.7 (primary), 19.3, 25.3, 30.5, 62.1, 63.2, 67.5 (secondary), 97.8, 120.7 (tertiary), 139.2 (quaternary); LR−CI MS (NH_3): *m/z* (relative intensity) 85.06 (100), 169.12 (56), 187.13 ($[M + H]^+$, 32); HR−CI MS: for $C_{10}H_{18}O_3$ $[M]^+$, calcd 186.1256, found 186.1260, for $C_{10}H_{19}O_3$ $[M + H]^+$, calcd 187.1334, found 187.1340.

(*E*)-4-(4′-Benzoylbenzyloxy)-1-[(tetrahydro-2H-pyran-2-yl)oxy]-3-methyl-2-butene (6a). Compound **5** (190 mg, 1.0 mmol) was dissolved in THF (2.0 mL) and cooled to 0 °C prior to sodium hydride (90 mg of 60% dispersion in oil, 2.3 mmol) addition. After 1 h, 4-benzoylbenzyl bromide[35] (450 mg, 1.6 mmol) was added and stirred for 1 h at 0 °C followed by 24 h at room temperature. The reaction mixture was poured over water and extracted with EtOAc. The combined extracts were dried over Na_2SO_4 and filtered. The filtrate was evaporated and the residue purified by flash chromatography on silica gel (toluene/EtOAc, 5:2, v/v). Evaporation of the solvent gave **6a** as a light yellow oil (300 mg, 78%). R_f 0.42 (silica gel, toluene/EtOAc, 5:2, v/v); ^{1}H NMR (300 MHz, $CDCl_3$): δ 1.53−1.86 (m, 6H), 1.78 (s, 3H), 3.53−3.57 (m, 1H), 3.89−3.92 (m, 1H), 4.02 (s, 2H), 4.13 (dd, 1H, J = 6.0, 12.0), 4.36 (dd, 1H, J = 6.0, 12.0), 4.59 (s, 2H), 4.68 (t, 1H, J = 3.6), 5.72 (t, 1H, J = 6.0), 7.49 (d, 2H, J = 6.0), 7.50 (t, 2H, J = 9.0), 7.61 (t, 1H, J = 6.0), 7.82 (d, 4H, J = 9.0); ^{13}C NMR (75.4 MHz, $CDCl_3$): δ 14.2 (primary), 19.6, 25.5, 30.7, 62.3, 63.3, 71.2, 75.9 (secondary), 98.1, 124.1, 127.2, 129.3, 130.0, 130.3, 132.4 (tertiary), 135.9, 136.7, 137.7, 143.3, 196.4 (quaternary); LR−FAB MS (MNBA): *m/z* (relative intensity) 167.1 (25), 195.1 (100), 279.5 (8), 297.2 (7), 381.2 ($[M + H]^+$, 2); LR−FAB MS: for $C_{24}H_{29}O_4$ $[M + H]^+$, calcd 381.2, found 381.2.

(*E*)-4-(3′-Benzoylbenzyloxy)-1-[(tetrahydro-2H-pyran-2-yl)oxy]-3-methyl-2-butene (6b). Compound **6b** was prepared and purified using the procedure described for the synthesis of **6a**. After chromatography, **6b** was obtained as a light yellow oil (260 mg, 68%). R_f 0.43 (silica gel, toluene/EtOAc, 5:2, v/v); ^{1}H NMR (200 MHz, $CDCl_3$): δ 1.52−1.83 (m, 6H), 1.71 (s, 3H), 3.45−3.55 (m, 1H), 3.81−3.91 (m, 1H), 3.95 (s, 2H), 4.07 (dd, 1H, J = 6.0, 12.0), 4.29 (dd, 1H, J = 6.0, 12.0), 4.52 (s, 2H), 4.62 (t, 1H, J = 4.0), 5.66 (t, 1H, J = 6.0), 7.46 (t, 1H, J = 8.0), 7.50 (t, 2H, J = 8.0), 7.56 (d, 1H, J = 6.0), 7.57 (t, 1H, J = 6.0), 7.69 (d, 1H, J = 8.0), 7.76 (s, 1H), 7.79 (d, 2H, J = 6.0); ^{13}C NMR (75.4 MHz, $CDCl_3$): δ 14.1 (primary), 21.3, 25.5, 30.7, 62.2, 63.2, 71.3, 75.7 (secondary), 98.0, 124.0, 127.6, 128.3, 129.0, 129.3, 130.0, 131.7, 132.4 (tertiary), 135.9, 137.5, 137.7, 138.9, 196.4 (quaternary); LR−FAB MS (MNBA): *m/z* (relative intensity) 165.1 (23), 195.2 (100), 279.2 (16), 298.2 (30), 381.2 ($[M + H]^+$, 3); LR−FAB MS: for $C_{24}H_{29}O_4$ $[M + H]^+$, calcd 381.2, found 381.2.

(*E*)-1-[(Tetrahydro-2H-pyran-2-yl)oxy]-3-methyl-4-*N*-phthalamido-2-butene (6c). To a stirred flask containing **5** (186 mg, 1.0 mmol), phthalimide (145 mg, 1.0 mmol), and PPh_3 (212 mg, 1.0 mmol) dissolved in 5.0 mL of THF was added a solution of DEAD (174 mg, 1.0 mmol) in 2.0 mL of THF dropwise over 30 min. The reaction was allowed to proceed for 18 h at room temperature at which time additional PPh_3 (106 mg) and DEAD (90 mg) were added. The mixture was then stirred for 24 h at room temperature followed by a third aliquot of the same quantities of PPh_3 and DEAD. After a final 18 h of reaction, hexane (10 mL) was added to the mixture to precipitate triphenylphosphine oxide and diethyl hydrazinedicarboxylate. The flask was stored overnight at 4 °C, and the solid byproducts were removed by filtration. The filtrate was evaporated, and the residue was applied to a silica gel column which was eluted with toluene/EtOAc (5:2, v/v) giving **6c** in 79% yield as white crystals. mp: 56−58 °C; R_f 0.57 (silica gel, toluene/EtOAc, 5:2, v/v); ^{1}H NMR (300 MHz, $CDCl_3$): δ 1.54−1.86 (m, 6H), 1.74 (s, 3H), 3.49−3.52 (m, 1H), 3.83−3.86 (m, 1H), 4.04−4.11 (m, 1H), 4.23−4.33 (m, 1H), 4.25 (s, 2H), 4.62 (t, 1H, J = 6.0), 5.55 (t, 1H, J = 6.0), 7.73−7.81 (m, 2H), 7.90−7.99 (m, 2H); ^{13}C NMR (75.5 MHz, DEPT, $CDCl_3$): δ 15.0 (primary), 19.4, 25.5, 30.6, 44.5, 62.2, 63.2 (secondary), 97.8, 123.4, 133.4, 134.0 (tertiary), 132.0, 133.9, 168.1 (quaternary); LR−FAB MS (MNBA): *m/z* (relative intensity) 154 (45), 214.2 (100), 232.2 (8), 316.2 ($[M + H]^+$, 12); HRFAB MS: for $C_{18}H_{22}NO_4$ $[M + H]^+$, calcd 316.1542, found 316.1569; NOE from H at C-2 (5.55 ppm) to H at C-4 (4.25 ppm): 1.7%; NOE from H at C-2 (5.55 ppm) to CH_3 at C-3 (1.74 ppm): 0.2%.

(*E*)-4-(4′-Benzoylbenzyloxy)-3-methyl-2-buten-1-ol (7a). To a solution of **6a** (380 mg, 1.0 mmol) in EtOH (6.0 mL) was added PPTs (25 mg, 0.10 mmol) and the reaction stirred at 55 °C for 8 h. The solvent was partially evaporated in vacuo, the resulting solution was diluted with Et_2O, and washed with half-saturated brine to remove the catalyst. The organic layer was dried over Na_2SO_4 and concentrated to yield **7a** (300 mg, 100%). R_f 0.29 (silica gel, toluene/EtOAc, 5:2, v/v); ^{1}H NMR (300 MHz, $CDCl_3$): δ 1.75 (s, 3H), 3.98 (s, 2H), 4.24 (d, 2H, J = 6.0), 4.57 (s, 2H), 5.73 (t, 1H, J = 9.0), 7.47 (d, 2H, J = 9.0), 7.49 (t, 2H, J = 6.0), 7.60 (t, 1H, J = 6.0), 7.80 (d, 4H, J = 9.0); ^{13}C NMR (75.4 MHz, $CDCl_3$): δ 14.1 (primary), 59.0, 71.2, 75.8 (secondary), 126.7, 127.2, 128.3, 130.0, 130.3, 132.5 (tertiary), 135.0, 136.7, 137.6, 143.3, 196.6 (quaternary); LR−FAB MS (MNBA): *m/z* (relative intensity) 167.2 (22), 195.2 (100), 211.1 (11), 279.2 (10), 289.2 (5), 297.2 ($[M + H]^+$, 5); HR−FAB MS: for $C_{19}H_{21}O_3$ $[M + H]^+$, calcd 297.1485, found 297.1484.

(*E*)-4-(3′-Benzoylbenzyloxy)-3-methyl-2-buten-1-ol (7b). The procedure described for the preparation of **7a** was used for the synthesis of **7b**. The product was obtained in 100% yield (300 mg). R_f 0.30 (silica gel, toluene/EtOAc, 5:2, v/v); ^{1}H NMR (300 MHz, $CDCl_3$): δ 1.70 (s, 3H), 3.95 (s, 2H), 4.21 (d, 2H, J = 6.0), 4.54 (s, 2H), 5.69 (t, 1H, J = 6.0), 7.46 (t, 1H, J = 6.0), 7.48 (t, 2H, J = 9.0), 7.58 (d, 1H, J = 9.0), 7.59 (t, 1H, J = 9.0), 7.71 (d, 1H, J = 9.0), 7.79 (s, 1H), 7.80 (d, 2H, J = 6.0); ^{13}C NMR (75.4 MHz, $CDCl_3$): δ 14.1 (primary), 58.9, 71.4, 75.7 (secondary), 126.7, 128.3, 128.4, 129.1, 129.4, 130.1, 131.7, 132.6 (tertiary), 135.0, 137.5, 137.7, 138.7, 196.8 (quaternary); LR−FAB MS (MNBA): *m/z* (relative intensity) 154 (45), 195.1 (100), 213.1 (10), 279.2 (17), 297.1 ($[M + H]^+$, 5); HR−FAB MS: for $C_{19}H_{21}O_3$ $[M + H]^+$, calcd 297.1485, found 297.1494.

(*E*)-4-(4′-Benzoylbenzyloxy)-3-methyl-2-buten-1-bromide (8a). To the alcohol **7a** (180 mg, 0.50 mmol) in CH_2Cl_2 (4.0 mL) were added CBr_4 (190 mg, 0.60 mmol) and PPh_3 (160 mg, 0.60 mmol). The reaction was stirred under N_2 for 4 h at room temperature. Hexanes were added to precipitate PPh_3O which was subsequently removed by filtration. The filtrate was concentrated under reduced pressure to afford the bromide in quantitative yield. R_f 0.97 (silica gel, toluene/EtOAc, 5:2, v/v); ^{1}H NMR (300 MHz, $CDCl_3$): δ 1.80 (s, 3H), 4.01 (s, 2H), 4.06 (d, 2H, J = 6.0), 4.58 (s, 2H), 5.87 (t, 1H, J = 9.0), 7.49 (t, 2H, J = 6.0), 7.51 (d, 2H, J = 6.0), 7.60 (t, 1H, J = 6.0), 7.82 (d, 4H, J = 9.0); ^{13}C NMR (75.4 MHz, $CDCl_3$): δ 13.7 (primary), 28.0, 71.4, 75.1 (secondary), 122.7, 127.2, 128.3, 130.0, 130.3, 132.4 (tertiary), 136.2, 138.0, 138.2, 142.9, 200.1 (quaternary); LR−FAB MS (MNBA): *m/z* (relative intensity) 195.2 (20), 279.2 (100), 359.0/361.0 ($[M + H]^+$, 3); HR−FAB MS: for $C_{19}H_{20}O_2Br$ $[M + H]^+$, calcd 359.0641, found 359.0652.

(*E*)-4-(3′-Benzoylbenzyloxy)-3-methyl-2-buten-1-bromide (8b). Compound **8b** was prepared from **7b** using the procedure outlined for the synthesis of **8a**. The desired bromide **8b** was obtained in quantitative yield. R_f 0.98 (silica gel,

toluene/EtOAc, 5:2, v/v); ^{1}H NMR (300 MHz, $CDCl_3$): δ 1.78 (s, 3H), 3.99 (s, 2H), 4.05 (d, 2H, J = 9.0), 4.56 (s, 2H), 5.85 (t, 1H, J = 9.0), 7.49 (t, 1H, J = 6.0), 7.50 (t, 2H, J = 6.0), 7.60 (d, 1H, J = 9.0), 7.59 (t, 1H, J = 9.0), 7.74 (d, 1H, J = 6.0), 7.81 (s, 1H), 7.83 (d, 2H, J = 9.0); ^{13}C NMR (75.4 MHz, $CDCl_3$): δ 13.7 (primary), 28.0, 71.5, 75.0 (secondary), 122.8, 128.3, 128.4, 128.7, 130.1, 131.6, 132.1, 132.5 (tertiary), 137.5, 137.7, 138.5, 138.9, 196.0 (quaternary); LR−FAB MS (MNBA): *m/z* (relative intensity) 195.2 (50), 279.2 (100), 359.0/361.0 ([M + H]$^+$, 8); HR−FAB MS: for $C_{19}H_{20}O_2Br$ [M + H]$^+$, calcd 359.0641, found 359.0649.

(*E*)-4-(4′-Benzoylbenzyloxy)-3-methyl-2-buten-1-diphosphate (3a). The allylic bromide **8a** (130 mg, 0.50 mmol) was pyrophosphorylated with $[(n\text{-Bu})_4N]_3HP_2O_7$ (1.1 g, 1.2 mmol) in anhydrous CH_3CN (4.0 mL) for 5 h at room temperature. The product was converted to the NH_4^+ salt using an ion-exchange column (Dowex 50W−X8 resin, NH_4^+ form) equilibrated in and eluted with 25 mM NH_4HCO_3/2-propanol (49:1, v/v), and the salt was obtained by lyophilization. The final product was purified employing a reversed-phase C_{18} column (Sep-pak cartridge) eluted with a step gradient containing 25 mM NH_4HCO_3 and CH_3CN. After lyophilization, **3a** (160 mg, 32%) was obtained as a white solid. R_f 0.56 (^{i}PrOH/NH_4OH/H_2O, 6:3:1, v/v/v); ^{1}H NMR (300 MHz, D_2O, adjusted to pH 8.5 with ND_4OD): δ 1.62 (s, 3H), 3.94 (s, 2H), 4.42 (t, 2H, J = 6.0), 4.51 (s, 2H), 5.63 (t, 1H, J = 6.0), 7.43 (d, 2H, J = 9.0), 7.44 (t, 2H, J = 9.0), 7.59 (t, 1H, J = 6.0), 7.66 (d, 4H, J = 6.0); ^{31}P NMR (121.4 MHz, D_2O, pH 8.5 with ND_4OD): δ −6.87 (d, 1P, J = 22), −10.79 (d, 1P, J = 23); UV (25 mM NH_4HCO_3): λ_{max} = 262 nm, ϵ = 17,100 M^{-1}·cm^{-1}; LR-ESI MS (CH_3OH/H_2O/TFA): *m/z* (relative intensity) − Ve mode, 455.0 ([M − H]$^-$, 100); + Ve mode, 242.2 (100), 279 (35), 457.1 ([M + H]$^+$, 17); HR-MALDI MS (DHBA/CH_3CN/H_2O/TFA): for $C_{19}H_{21}O_9P_2$ [M−H]$^+$, calcd 455.0653, found 455.0669; 97% chemical purity based on HPLC integration analysis. HPLC analysis was performed with a C_{18} Phenomenex Luna column (250 × 4.6 mm) eluted with a flow rate of 0.4 mL/min using a gradient of solvent A (25 mM NH_4HCO_3) and solvent B (CH_3CN) and detecting at 262 nm. Elution was performed by isocratic elution with 20% solvent B for 10 min followed by a 25 min linear gradient to 60% solvent B and finally a 5 min linear gradient to 100% solvent B with isocratic elution at 100% B for 10 min. Under these conditions, **3a** eluted at 25.1 min.

(*E*)-4-(3′-Benzoylbenzyloxy)-3-methyl-2-buten-1-diphosphate (3b). The allylic bromide **8b** was pyrophosphorylated as described for the preparation of **3a** to give **3b** as a white powder (150 mg, 30%). R_f 0.58 (^{i}PrOH/NH_4OH/H_2O, 6:3:1, v/v/v); ^{1}H NMR (300 MHz, D_2O, adjusted to pH 8.5 with ND_4OD): δ 1.54 (s, 3H), 3.86 (s, 2H), 4.35 (t, 2H, J = 6.0), 4.41 (s, 2H), 5.54 (t, 1H, J = 6.0), 7.39 (t, 4H, J = 6.0), 7.54 (d, 2H, J = 6.0), 7.59 (d, 2H, J = 9.0), 7.63 (s, 1H); ^{31}P NMR (121.4 MHz, D_2O, pH 8.5 with ND_4OD): δ −6.89 (d, 1P, J = 22), −10.81 (d, 1P, J = 22); UV (25 mM NH_4HCO_3): λ_{max} = 260 nm, ϵ = 26,000 M^{-1}·cm^{-1}; LR-ESI MS (CH_3OH/H_2O/TFA): *m/z* (relative intensity) − Ve mode, 219.5 (31), 245.0 (16), 454.9 ([M − H]$^-$, 100); + Ve mode, 242.2 (100), 279 (76), 457.0 ([M + H]$^+$, 26); HR-MALDI MS (DHBA/CH_3CN/H_2O/TFA): for $C_{19}H_{21}O_9P_2$ [M − H]$^+$, calcd 455.0653, found 455.0654; 72% chemical purity based on HPLC integration analysis using the conditions described for **3a**. Under these conditions, **3b** eluted at 25.1 min. The major impurity eluting at 43.6 min (22% based on integration) present in **3b** is the alcohol **7b** or isomer thereof.

[α,*β*(n)^{32}P]-(*E*)-4-(4′-Benzoylbenzyloxy)-3-methyl-2-buten-1-diphosphate ([^{32}P]3a). Alcohol **7a** (1.9 mg, 6.3 μmol) was reacted with anhydrous [^{32}P]H_3PO_4 (1.2 mg, 13 μmol) in CH_3CN (200 μL) containing 20% (v/v) CCl_3CN and triethylamine (2.5 mg, 26 μmol) for 2 h. The volatile components from the reaction were evaporated, and the resulting residue purified by reversed-phase chromatography using a C_{18} Sep-pak cartridge employing a NH_4HCO_3/CH_3CN stepwise gradient. The product [^{32}P]**3a** was obtained in 16% yield (specific activity 2100 Ci/mol); the concentration of solutions containing [^{32}P]**3a** were determined by UV using the wavelengths and extinction coefficients reported for **3a**. The radiochemical purity of [^{32}P]**3a** was assessed by thin-layer chromatography in ^{i}PrOH/NH_4OH/H_2O (6:3:1, v/v/v) followed by phosphorimaging analysis and was found to be 35%. The sample also contained 32% monophosphate, 23% triphosphate, and 10% inorganic phosphate.

[α,*β*(n)^{32}P]-(*E*)-4-(3′-Benzoylbenzyloxy)-3-methyl-2-buten-1-diphosphate ([^{32}P]3b). Compound [^{32}P]**3b** was prepared as described above for [^{32}P]**3a**. After reversed-phase chromatography, [^{32}P]**3b** was obtained in 1% yield (specific activity 1300 Ci/mol) and 76% radiochemical purity. The amount of inorganic phosphate was 24%.

***N*-Dansyl-GC(4-BBDMA)VIA (10a).** Compound **10a** was prepared by reacting **8a** with **9** under acidic conditions containing DMF/butanol/0.025% TFA (2:1:1, v/v/v) and 1 M $Zn(OAc)_2$ as a catalyst following the procedure described by Xue et al.[40] The crude product was purified by reversed-phase HPLC employing a H_2O/CH_3CN (containing 0.2% TFA) gradient: ESI MS and ESI MS/MS were obtained. ESI MS for $C_{50}H_{64}O_{10}N_6S_2$ [M]$^+$, calcd 972.41, found 971.99 ± 0.57, $C_{50}H_{65}O_{10}N_6S_2$ [M + H]$^+$, calcd 973.4, found 973.2, $C_{50}H_{66}O_{10}N_6S_2$ [M + 2H]$^{2+}$, calcd 487.2, found 487.0; UV (H_2O/CH_3CN/TFA, 50/50/0.2) λ_{max} = 320 nm, ϵ = 1780 M^{-1}·cm^{-1}; fluorescence (H_2O/CH_3CN/TFA, 50/50/0.2) λ_{ex} = 322 nm, λ_{em} = 530 nm, intensity = 0.37 (relative to *N*-dansylglycine, 1.0).

***N*-Dansyl-GC(3-BBDMA)VIA (10b).** Compound **10b** was prepared from **8b** and **9** as described for **10a**: ESI MS and ESI MS/MS were obtained. ESI MS for $C_{50}H_{64}O_{10}N_6S_2$ [M]$^+$, calcd 972.41, found 972.17 ± 0.31, $C_{50}H_{65}O_{10}N_6S_2$ [M + H]$^+$, calcd 973.4, found 973.2, $C_{50}H_{66}O_{10}N_6S_2$ [M + 2H]$^{2+}$, calcd 487.2, found 487.0; UV (H_2O/CH_3CN/TFA, 50/50/0.2) λ_{max} = 320 nm, ϵ = 1780 M^{-1}·cm^{-1}; fluorescence (H_2O/CH_3CN/TFA, 50/50/0.2) λ_{ex} = 322 nm, λ_{em} = 530 nm, intensity = 0.24 (relative to *N*-dansylglycine, 1.0).

Purification of yPFTase and hPGGTase-I. yPFTase was purified as described by Mayer et al.[45] and published in our earlier work.[28] hPGGTase-I was purified using modifications of published procedures.[19,46,47]

Enzyme Assays. A spectrophotometric assay was employed to monitor yPFTase activity as previously described by Gaon et al.[28] modified from the original published procedure.[38,39]

Substrate Studies. Large-scale enzymatic reactions were performed to determine if **3a** and **3b** were alternate substrates for yPFTase and hPFTase. The reactions (10 mL) contained 10 μM **3a** or **3b**, 45 nM yPFTase, or 100 nM hPFTase, and other assay components at the same concentration omitting the natural substrate, **1**, and detergent, *n*-dodecyl-*β*-D-maltoside. The reactions were desalted and concentrated by applying to a Sep-pak C_{18} cartridge. The samples were washed with H_2O/CH_3CN/TFA (95:5:0.2, v/v/v) and eluted with CH_3CN/TFA (100:0.2, v/v). The fluorescent fractions were concentrated in vacuo, dissolved in H_2O/CH_3CN/TFA (50:50:0.2, v/v/v), and purified by HPLC using a reversed-phase C_{18} column with a H_2O/CH_3CN/TFA gradient. The product peaks were collected and analyzed by ESI MS and ESI MS/MS.

Enzyme Inhibition Experiments. To determine if **3a** and **3b** were competitive inhibitors of yPFTase and hPFTase, duplicate assays were run in which the natural substrate, **1**, was maintained at fixed concentrations (1.0, 1.5, 3.0, 7.0 μM), and **3a** (0, 3.0, 6.0, 9.0, 12 μM) or **3b** (0, 1.0, 2.0, 3.0, 4.0 μM) for yPFTase; **3a** or **3b** (0, 1.0, 2.0, 3.0, 4.0 μM) for hPFTase were varied at each substrate concentration. The analogue concentrations were chosen based on their IC_{50} values performed first. The concentration of yPFTase and hPFTase in these experiments were 2.5 nM and 25 nM, respectively. The reaction rates were determined from initial velocity measurements using the fluorescence assay and K_i values were

(44) Das, N. P.; Allen, C. M. *Biochem. Biophys. Res. Commun.* **1991**, *181*, 729−735.
(45) Mayer, M. P.; Prestwich, G. D.; Dolence, J. M.; Bond, P. D.; Wu, H.-Y.; Poulter, C. D. *Gene* **1993**, *132*, 41−47.
(46) Zhang, F. L.; Diehl, R. E.; Kohl, N. E.; Gibbs, J. B.; Giros, B.; Casey, P. J.; Omer, C. A. *J. Biol. Chem.* **1994**, *269*, 3175−3180.
(47) Stirtan, W. G.; Poulter, C. D. *Arch. Biochem. Biophys.* **1995**, *321*, 182−190.

calculated from Eadie-Hofstee plots obtained from a Macintosh PowerMac G3 computer running Kaleidagraph (v. 3.0.1) software.

X-ray Crystallographic Studies. Crystals of the FPT:**3a** complex were prepared by soaking **3a** into preformed crystals using methods previously described.[41] X-ray diffraction data were collected on a Rigaku rotating anode generator equipped with osmic mirrors and a Raxis-IV image plate detector. With the detector set at 135 mm, data were collected in 236 contiguous 0.30° oscillation images each exposed for 9 min. The data extend to 2.1 Å resolution and have a R_{merge} of 3.5% with a 4.4-fold multiplicity. The structure was refined using XPLOR98.1 (Molecular Simulations Inc.) to an R_{factor} of 19.9%. [A figure showing the electron density contoured at 1.0σ for **3a** can be found in the Supporting Information section.]

Photoinactivation Studies. Photolysis reactions were performed in silanized quartz test tubes (10 × 45 mm) and contained 52 mM Tris·HCl pH 7.0, 5.8 mM DTT, 12 mM $MgCl_2$, 12 μM $ZnCl_2$, 25 mM NH_4HCO_3, 13 μM **3a** or 6.6 μM **3b** which were chosen to be 10-fold above their K_i values, and 3.8 nM yPFTase in a final volume of 0.75 mL. For substrate protection studies, **1** was added at a final concentration of 100 μM. All reactions were photolyzed at 350 nm for up to 12 h using a UV Rayonet minireactor equipped with 8 RPR-3500° lamps and a circulating platform at 4 °C. At various photolysis times, 50 μL aliquots were removed, placed on ice, and assayed for activity.

Photolysis Reaction of Prenyltransferases with [^{32}P]-3a and [^{32}P]3b. The photolysis reactions (100 μL) were performed in silanized quartz test tubes (10 × 45 mm) and contained 52 mM Tris·HCl pH 7.0, 5.8 mM DTT, 12 mM $MgCl_2$, 12 μM $ZnCl_2$, 25 mM NH_4HCO_3, 13 μM [^{32}P]**3a** or 6.6 μM [^{32}P]**3b**, and 380 nM enzyme (yPFTase, hPFTase, hPGG-Tase-I). For substrate protection studies, **1** or **2** was added to a final concentration of 100 μM. Reactions were irradiated for 2 h using the above apparatus. Loading buffer (50μL; 4% SDS, 12% glycerol (m/v), 50 mM Tris, 2% mercaptoethanol (v/v), 0.01% bromophenol blue) was then added to each sample, samples were heated to 70 °C for 5−10 min, and analyzed by SDS−PAGE with a 10% Tris-tricine gel. Gels were silver stained and exposed to a phosphorimaging screen for 14−22 h. The relative intensities of photolabeled products were determined by phosphorimaging analysis.

Photolysis Reaction of FPP Synthase with [^{32}P]3a and [^{32}P]3b. The photolysis reactions were accomplished as described above with the prenyltransferases except 470 nM FPP synthase was used, and substrate protection studies were completed with **1** at 100 μM. Reactions were irradiated for 2 h using the same apparatus. Loading buffer was then added to each sample, samples were heated to 70 °C for 5−10 min, and analyzed by SDS−PAGE with a 10% Tris-tricine gel. Gels were silver stained and exposed to a phosphorimaging screen for 42 h. The relative intensity of photolabeled products were determined by phosphorimaging analysis.

Acknowledgment. The authors would like to thank Dr. Leo Bonilla and Nancy Raha, University of Minnesota Cancer Institute, for obtaining the mass spectral data. This research was supported by funds from the American Cancer Society (BE-222 and JFRA-584) and the National Institutes of Health (GM58842).

Supporting Information Available: Copies of ^{1}H NMR, ^{31}P NMR and mass spectral data for **3a** and **3b** and intermediates in their syntheses as well as HPLC chromatograms of **3a** and **3b** are included. Plots of photoinactivation kinetics, photolabeling efficiencies, and a figure showing the electron density for **3a** from the rPFTase−**3a** complex contoured at 1.0σ are also enclosed. This material is available free of charge via the Internet at http://pubs.acs.org.

JO991130X